Evaluation of SMAP and CYGNSS Soil Moistures in Drought Prediction Using Multiple Linear Regression and GLDAS Product

Komi Edokossi, Shuanggen Jin, Andres Calabia, Iñigo Molina, and Usman Mazhar

Abstract

Drought is a devastating natural hazard and exerts profound effects on both the environment and society. Predicting drought occurrences is significant in aiding decision-making and implementing effective mitigation strategies. In regions characterized by limited data availability, such as Southern Africa, the use of satellite remote sensing data promises an excellent opportunity for achieving this predictive goal. In this study, we assess the effectiveness of Soil Moisture Active Passive (SMAP) and Cyclone Global Navigation Satellite System (CYGNSS) soil moisture data in predicting drought conditions using multiple linear regression–predicted data and Global Land Data Assimilation System (GLDAS) soil moisture data. SMAP and CYGNSS data exhibit strong spatiotemporal congruence with the predicted soil moisture data. Pearson correlation coefficients further underscore this consistency, with correlations of r = 0.78 between GLDAS and SMAP, r = 0.61 between GLDAS and CYGNSS, and r = 0.84 between GLDAS and the estimated soil moisture. The proficient performance of SMAP and CYGNSS soil moisture data in tandem with other variables underscores their efficacy in predicting drought conditions.

Introduction

Drought constitutes a significant natural hazard characterized by prolonged periods of low precipitation and elevated temperatures, leading to heightened evapotranspiration rates (Jin and Zhang 2016; Huang and Jin 2020; Elameen *et al.* 2023). This climatic phenomenon directly impacts agricultural yields due to deficits in soil moisture (Marsh, 2007; Dai 2011). Within the context of the Southern Africa region, the effect of recent drought events, spanning from 2015–2016 to 2018–2020, has been particularly profound. These occurrences have exacted a heavy toll on both human livelihoods and crop yields. For instance, during the drought of 2015–2016, crop production underwent a precipitous decline of up to 66%, concurrently affecting over a quarter of the region's population (Ainembabazi, 2018). During 2018–2019, the drought affected more than 40% of the population (Johannesburg Regional Bureau 2020), and the crop production was 10% below the average (World Food Program 2019).

The scientific literature commonly recognizes four distinct categories of drought (Mishra and Singh 2010): meteorological, agricultural, hydrological, and socioeconomic. Meteorological drought manifests as an insufficient occurrence of precipitation over a given time span—whether short or prolonged—resulting in a deficit of soil moisture that adversely affects plants, giving rise to what is termed agricultural drought. Hydrological drought materializes when there is an insufficiency in water availability across streams, reservoirs, and groundwater sources. In contrast, socioeconomic drought pertains to the inability of water supply to adequately meet demand (Mishra and Singh 2010).

The prediction of drought occurrences plays a pivotal role in facilitating early warnings and mitigating their subsequent effects. Over time, numerous methodologies and formulations have been developed and used to achieve this objective. The predominant approaches comprise statistical methods and dynamical methods, which harness climate and/or hydrologic models to simulate the intricate physical processes of the atmosphere, land, and oceans (Hao *et al.* 2018). Within the realm of statistical methods, a spectrum of techniques is embraced, including time series models, regression models, artificial intelligence models, Markov chain models, and conditional probability models. These methodologies stand out as extensively used avenues. In the context of statistical methodologies, the identification of appropriate predictors derived from atmospheric, terrestrial, and oceanic domains, as well as the determination of predictands for the target timeframe, is of paramount importance (Hao *et al.* 2018). For instance, the efficacy of time series models predominantly hinges on the persistence of certain indicators, which serves as the bedrock for achieving accurate predictions. The autoregressive integrated moving average technique emerges as an exceptionally apt choice for prediction within climatology and hydrology, as it effectively handles linear relationships between predictors and predictands, albeit without capturing nonlinearity. In the realm of statistical prediction, the conventional linear regression method finds applications in hydrology and climatology. This method establishes a linear connection between the predictand and suitable predictors, representing the simplest avenue for climatohydrological prediction. The modeling of the association between drought indices and predictors often uses the regression model (Barros and Bowden 2008; Liu and Juárez 2001; Panu and Sharma 2002; Sun *et al.* 2012). In scenarios in which nonlinear relationships are at play, the locally weighted polynomial regression offers a valuable alternative for modeling associations (Hwang and Carbone 2009; Liu and Hwang

Komi Edokossi is with the School of Remote Sensing and Geomatics Engineering, Nanjing University of Information Science and Technology, Nanjing 210044, China.

Shuanggen Jin is with the School of Remote Sensing and Geomatics Engineering, Nanjing University of Information Science and Technology, Nanjing 210044, China; the Shanghai Astronomical Observatory, Chinese Academy of Sciences, Nanjing 210044, China; and the School of Surveying and Land Information Engineering, Henan Polytechnic University, Nanjing 210044 (sgjin@nuist.edu.cn).

Andres Calabia is with the Department of Physics and Mathematics, University of Acala, Nanjing 210044.

Iñigo Molina is with the School of Remote Sensing and Geomatics Engineering, Nanjing University of Information Science and Technology, Nanjing 210044; and the School of Land Surveying, Geodesy and Mapping Engineering, Universidad Politécnica de Madrid, Nanjing 210044.

Usman Mazhar is with the School of Remote Sensing and Geomatics Engineering, Nanjing University of Information Science and Technology, Nanjing 210044.

Corresponding author: Shuanggen Jin (sgjin@nuist.edu.cn)

Contributed by Prasad S. Thenkabail, October 13, 2023 (sent for review November 8, 2023; reviewed by Itiya Aneece, Xiaodong Li, Xutong Niu).

Photogrammetric Engineering & Remote Sensing
Vol. 90, No. 5, May 2024, pp. 303–312.
0099-1112/22/303–312

doi: 10.14358/PERS.23-00075R2

2015). Given the intricate interplay among hydroclimatic variables, artificial intelligence (AI), with its nonlinear capabilities, has emerged as a preferable tool for climatohydrological prediction over linear models. Among these models, the artificial neural network, support vector regression, or support vector machine, fuzzy logic, wavelet transformation, and genetic algorithm or genetic programming are the most used (Bourdin *et al.* 2012; Fahimi *et al.* 2017; Nourani *et al.* 2014; Rhee and Im 2017; Wang, Chau *et al.* 2009; Yaseen *et al.* 2015). The artificial neural network (Mishra *et al.* 2007; Mishra and Desai 2006; Morid *et al.* 2007), wavelet transformation (Maity *et al.* 2016; Ozger *et al.* 2011), and support vector machine (Ganguli and Reddy 2014) have been used for prediction within climatology and hydrology. For Markov chain prediction, drought is classified in dry and wet states with specific thresholds (Lawrimore *et al.* 2002; Steinemann and Cavalcanti 2006; Svoboda *et al.* 2002; Zink *et al.* 2016). The prediction of hydroclimatic variables using the joint distribution of conditional probability model has been used in several studies (Khedun *et al.* 2014; Liu and Hwang 2015; Wang, Robertson *et al.* 2009; Wu *et al.* 2011; Yan *et al.* 2012). In addition, Qiu *et al.* (2003) used the multiple linear regression (MLR) method with meteorological data to predict soil moisture deficit in the Danangou catchment in the Loess Plateau of China with an error of 2% only. Furthermore, soil moisture strengthened or weakened drought severity (Koster *et al.* 2017; Schubert *et al.* 2007; Su and Dickinson 2017; Yuan and Wood 2013) can contribute to very realistic prediction (Evans *et al.* 2017; Koster *et al.* 2004; Nicolai-Shaw *et al.* 2016; Seneviratne *et al.* 2010).

Studies using Soil Moisture Active Passive (SMAP) soil moisture estimates have reported their excellent suitability for drought monitoring. For instance, Mishra *et al.* (2017) used SMAP data and the soil water deficit index to quantify agricultural drought over the United States. The authors found their method a very effective scheme for agricultural drought monitoring. Zhu *et al.* (2019) assessed SMAP derived soil water deficit index for agricultural drought monitoring in Xiang River Basin, China, using the Pearson correlation. Their results showed good performance of SMAP in drought monitoring. In addition, SMAP-derived standardized soil moisture index (SSI) was used to monitor drought in the Southeast of the United States by Xu *et al.* (2018). They concluded that SSI was effective for short-term drought monitoring after validation. Eswar *et al.* (2018) investigated drought monitoring over the United States using SMAP and verified its performance for analyzing the responses to changes in drought conditions.

In an effort to elucidate the intricate relationships among hydrometeorological variables, (Nicolai-Shaw *et al.* 2017) used remote sensing data to extract composite drought indices. Their investigation unveiled the prominence of precipitation deficits as a pivotal driver of negative soil moisture conditions. Through their study, they revealed noteworthy anomalies in precipitation, temperature, and evapotranspiration, with observable delays in the response of vegetation indices during the zenith of arid periods. Using observations of terrestrial water storage gleaned from the Gravity Recovery and Climate Experiment (GRACE). Terrestrial water storage observations from GRACE was used by Thomas *et al.* (2014) to measure hydrological drought occurrence and severity in the Amazon and Zambezi River basins and the southeastern United States and Texas (Heki and Jin 2023). In addition, global navigation satellite system reflectometry also provides soil mositure and drought monitoring (Jin *et al.* 2011; Edokossi *et al.* 2020; Najibi and Jin 2013; Calabia *et al.* 2020; Qian and Jin 2016), particularly the space-borne Cyclone Global Navigation Satellite System (CYGNSS).

Despite the prevalence of works focused on the utility of SMAP and CYGNSS soil moisture data in drought monitoring, fewer studies have delved into their potential for drought prediction. Qiu *et al.* (2003) used MLR and meteorological factors for spatiotemporal estimate of soil moisture in a small catchment of the Loess plateau in China and found the model useful. Jung *et al.* (2017) used Moderate Resolution Imaging Spectroradiometer (MODIS) land surface temperature (LST) and normalized difference vegetation index (NDVI) and precipitation with the MLR method to estimate spatial soil moisture in South Korea. MLR models were used with land use and terrain indices to predict soil moisture spatially by Qiu *et al.* (2010). Prakash *et al.* (2018) used machine learning techniques such as multiple linear regression, support vector regression, and recurrent neural networks for prediction of soil moisture and found that MLR performed well. Drought prediction stands as a crucial information source for decision makers, facilitating early warnings and bolstering disaster mitigation efforts. Within the realm of agricultural drought prediction, the intrinsic complexity of hydrological processes, particularly on a global scale, renders the task notably more challenging than monitoring alone. Nevertheless, SMAP and CYGNSS exhibit a host of advantages over traditional measurement methods. They encompass global coverage, operability under diverse weather conditions, and high spatiotemporal resolution, to name a few.

This study aims to assess the predictive capabilities of SMAP and CYGNSS soil moisture data. This assessment is achieved through a comprehensive comparison and validation process against both MLR predicted soil moisture and the Global Land Data Assimilation System (GLDAS) soil moisture data set and the Southern African drought map of the same period. The objectives of this research are twofold. The first is to estimate soil moisture using the MLR method in conjunction with climatometeorological variables. Soil moisture is estimated through the application of the MLR method, leveraging commonly used climatometeorological variables such as precipitation, evapotranspiration, and total water storage. The second objective is to elucidate the spatiotemporal evolution of SMAP and CYGNSS soil moisture data during the 2018–2019 time frame. A critical aspect of the study involves the meticulous evaluation of the performance of SMAP and CYGNSS soil moisture data in drought prediction, achieved through comparative analyses with other soil moisture (GLDAS and MLR) data sets and a Southern African drought map.

This paper is structured as follows: "Study Area" provides a detailed description of the study geography, while data and methods are presented in the next section. "Results and Analysis" presents the findings, which are subsequently dissected and contextualized with in "Discussion." Finally, conclusions are given in the last section.

Study Area

Southern Africa as the study area is underpinned by the region's recurrent susceptibility to drought, which significantly affects the local populace. A notable instance of this occurred during the 1994–1995 period, when severe droughts afflicted a majority of southern African nations (Edokossi *et al.*, 2020). This phenomenon was particularly pronounced in the northwestern part of Zimbabwe, where the 1994–1995 season experienced rainfall levels near historical lows. Additionally, the 2015–2016 El Niño event led to life-threatening extreme weather across various global regions, including several African nations. However, a pivotal reason motivating this geographical choice stems from the region's ongoing struggle with drought, notably spanning from 2018 to 2020 (GDACS 2020). The 2018–2019 season was characterized by a drought that commenced in late October 2018, coinciding with the planting period. This event was classified as a level 2 red-class occurrence by the Global Disaster Alert and Coordination System (GDACS), posing substantial challenges to food security and plunging millions into conditions of food insecurity. Similarly, the 2019–2020 season exhibited rainfall levels below the historical average from mid-October to mid-December, accompanied by persistent dry conditions that impeded the planting season (Relief Web 2020).

The choice of the 2018–2019 period can be attributed to the availability of SMAP and CYGNSS satellite data covering the region. Although SMAP and CYGNSS commenced data recording in 2015 and 2017, respectively, their data were not universally accessible for this specific period. To visualize the study area and major vegetation biomes, seasonally averaged mean rainfall anomalies and seasonally averaged mean temperature anomalies, Figures 1, 2, and 3 provide a comprehensive depiction.

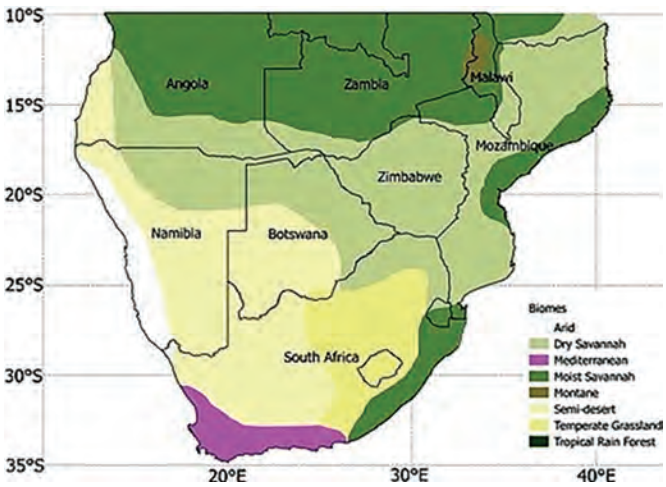

Figure 1. Map of the study area with major vegetation biomes (Lawal *et al.* 2019).

Figures 2 and 3 show the seasonally averaged mean rainfall anomalies and temperature anomalies from 1981 to 2010, respectively. The maps depicted the similar spatial distribution for 2018–2019 for both variables. Furthermore, the spatial distribution of rainfall and temperature anomalies reflect the spatial distribution of major vegetation biomes, denoting the overall climatic characteristics of the study area.

Data and Methods

Data Sets

This research leverages satellite soil moisture (SM) observations spanning from 2018 to 2019, sourced from both the SMAP and CYGNSS missions (Table 1). In conjunction with these, complementary data sets such as evapotranspiration (ET), total water storage (TWS), GLDAS Noah model SM, and rainfall data are also incorporated (see Table 1). The selection of these data sets is informed by their widespread use in climate–meteorological investigations of drought.

The SMAP mission, launched by the National Aeronautics and Space Administration (NASA) in January 2015, plays a pivotal role in supplying global measurements of soil moisture levels and freeze/thaw states (Entekhabi *et al.* 2010). This mission uses an ensemble of an L-band radar and an L-band radiometer, enabling the comprehensive mapping of soil moisture at a spatial resolution of 10 km. The revisit

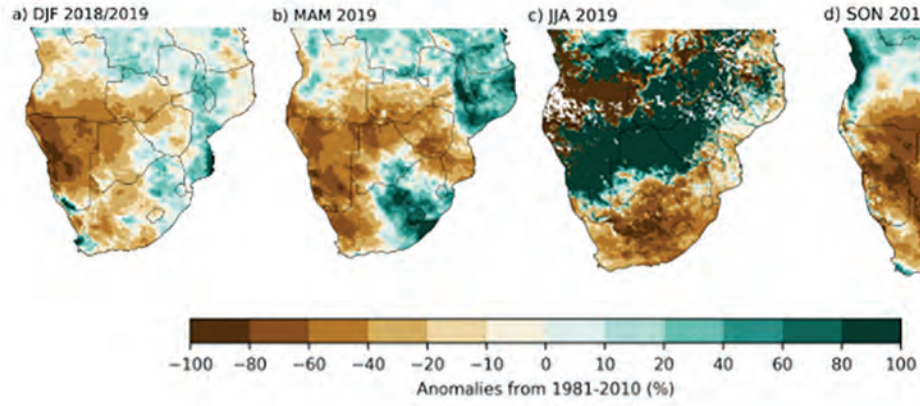

Figure 2. Seasonally averaged mean rainfall anomalies (percentage of mm/day) from 1981 to 2010 in Southern Africa (Source: Climate Hazards Group InfraRed Precipitation with Station [CHIRPS]). DJF = December to February; MAM = March to May; JJA = June to August; SON = September to November (Pinto 2020).

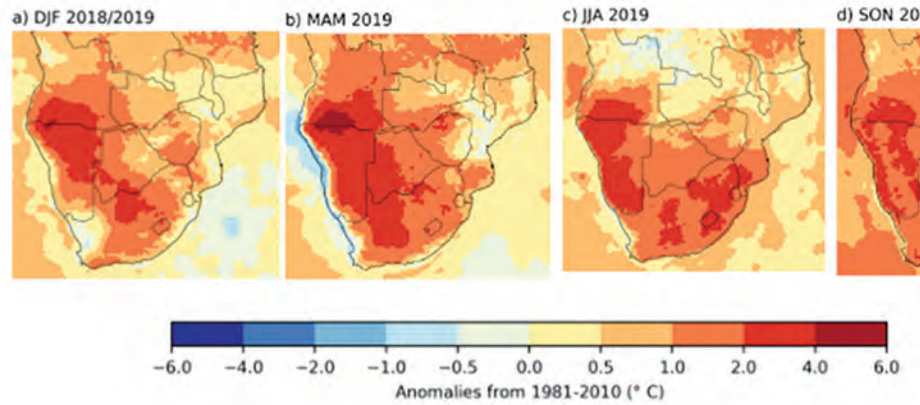

Figure 3. Seasonally averaged mean temperature anomalies (°C) from 1981 to 2010 in Southern Africa. (a) DJF 2018/19. (b) MAM 2019. (c) JJA 2019. (d) SON 2019. (Source: ERA5). DJF = December to February; MAM = March to May; JJA = June to August; SON = September to November (Pinto 2019).

Table 1. Data used in the study.

Sensors and Products	Parameter	Drought Type	Year	Spatial Resolution	Temporal Resolution
MOD16A2 V006 (MODIS)	ET	Ecological drought	2018–2019	500 m	8 day
L3SMAP-L-BAND RADIOMETER (SMAP)	SM	Agricultural drought	2018–2019	9 km	Daily
CYGNSS Level 3 (CYGNSS)			2018–2019	0.3° × 0.37°	1 day
GLDAS (NOAH model)			2018–2019	0.25° × 0.25°	Monthly
GRACE and GRACE-FO	TWS (LWE)	Hydrological drought	2018–2019	1° × 1°	Daily
TRMM (TMPA/3B43)	Rainfall	Meteorological drought	2018–2019	0.25° × 0.25°	Monthly

ET = evapotranspiration; SM = soil moisture; TWS = total water storage. LWE = Liquid water equivalent.

time spans 2–3 days, encompassing both clear and cloudy sky conditions. By fusing radar and radiometer measurements, SMAP extends the capability of delivering high-resolution soil moisture data. This is achieved by combining radiometer-derived soil moisture retrieval, offering elevated accuracy albeit coarser spatial resolution (40 km), with radar data (1–3 km) of finer resolution albeit lower retrieval accuracy. This integration affords the estimation of soil moisture across a diverse array of vegetation conditions (Entekhabi *et al.* 2010). For the SMAP data set, the Enhanced L3 version 4 soil moisture (SPL3SMAP) was used (Entekhabi *et al.* 2016). This L3SMAP data set is a composite amalgamation of daily global land surface condition estimates. The primary parameter is the surface soil moisture (typically representative of the top 5 cm, measured in cm^3/cm^3), presented on a global 9 km EASE-Grid 2.0, formatted as a Geotiff (Entekhabi *et al.* 2016).

CYGNSS, specializing in surface remote sensing, is primarily designed to measure ocean surface wind across all precipitation conditions. Comprising eight microsatellites, CYGNSS facilitates targeted observations with an average revisit interval of approximately 7 hours. With an inclination of 35° relative to the equator, it spans latitudes between approximately 38° N and 38° S. The CYGNSS level 3 version 1.0 SM data set, ranging from 0- to 5-cm depth and featuring a spatial resolution of 0.3° (latitude) × 0.37° (longitude), is used (CYGNSS 2020). Presented in volumetric water content (cm^3/cm^3), the data are archived daily in netCDF-4 format.

GLDAS encompasses four land surface models (Mosaic, Noah, the Community Land Model, and the Variable Infiltration Capacity) operating at global resolutions spanning from 2.5° to 1 km. With a temporal resolution of 3-hourly, data is subsequently aggregated to yield monthly products. GLDAS soil moisture data is particularly well-suited as a reference owing to its accuracy and extensive global coverage. Using advanced land surface modeling and data assimilation techniques, GLDAS achieves optimal generation of land surface state and flux fields. For this study, the GLDAS Noah Land Surface Model (LSM) L4 monthly 0.25 × 0.25° version 2.1 (GLDAS_NOAH025_M) data set, capturing top 10-cm soil moisture, serves as the reference. This data set, reprocessed in January 2020, supersedes its predecessor and is obtained from the main production stream. The archived data is disseminated in NetCDF format. Importantly, the GLDAS-2.1 products surpass their corresponding GLDAS-1 counterparts (Beaudoing and Rodell 2019).

The TWS derived from GRACE and its Follow-on (GRACE-FO) stands as a hydrological drought indicator, measuring alterations in water thickness near the Earth's surface. Launched in March 2002, GRACE-FO furnishes temporal gravity field measurements on a global scale. Designed to track Earth's mass shifts and alterations, particularly those associated with water, GRACE-FO, launched on 21 May 2018, plays a pivotal role in groundwater monitoring. Given the exacerbation of drought conditions due to climate change, there is a heightened reliance on groundwater for various purposes, notably agriculture, necessitating effective monitoring. The data set used for this study, GRACE/GRACE-FO RL06 v02 Mascon Grids with Corrections Applied, originates from the Center for Space Research (CSR) in Austin, Texas. This data set spans from April 2002 to December 2022 and is presented in NetCDF format (Save *et al.* 2016).

Rainfall data serves as a basis for comparative analysis with soil moisture content variations. This data set comprises three distinct products, each characterized by varying temporal resolutions: three-hourly (3B42), daily (3B42 derived), and monthly (3B43). The spatial resolution for these products is 0.25° × 0.25°, spanning latitudes from 50° S to 50° N. For this study, solely the TRMM 3B43 product for the 2018-2019 time frame is used, representing the monthly mean of the TRMM 3B42 data set (Tropical Rainfall Measuring Mission 2011).

Additionally, the MODIS16A2 version 6 evapotranspiration data set is harnessed, originating from the NASA/EOS project. This data set aids in the estimation of land surface evapotranspiration through the assimilation of MODIS and global meteorological data. The data set encompasses transpiration by vegetation, as well as evaporation from soil and canopy surfaces. It plays a pivotal role in furnishing information pertinent to regional water and energy balances, soil water statuses, and water resource management. Moreover, the long-term evapotranspiration data assist in quantifying the effects of shifts in land use, ecosystems, and climate on regional water resources and land surface energy changes (https://lpdaac.usgs.gov/products/mod16a2v006/). The product includes 8-day, monthly, and annual global ET, latent heat flux (LE), potential evapotranspiration (PET), potential latent heat flux (PLE), and 8-day, annual quality control (ET_QC) at a spatial resolution of 500 m (https://lpdaac.usgs.gov/products/mod16a2v006/).

Selected for their critical roles as hydrometeorological variables and drought indicators, the inclusion of precipitation, ET, and TWS lends comprehensive insights to this study. Furthermore, all the data used in this study and summarized in Table 1 are selected based on their availability over the study period for the study area.

Methods

In this paper, the capability of SMAP and CYGNSS soil moisture in drought prediction was evaluated. This was achieved through comparison and validation against GLDAS (reference soil moisture) and a Southern Africa drought map (considered as a ground truth map), and the estimated soil moisture obtained from some well known hydrological variables. First, for the estimate of the soil moisture, the MLR technique is harnessed to establish a robust relationship between independent variables (P, ET, and TWS) and the target variable (predicted soil moisture). MLR leverages the principle of least squares, seeking the best fit that minimizes the sum of squared residuals, thereby yielding an effective means of characterizing the association. The process of comparing predictors and validating their effectiveness encompasses two crucial steps. Initially, the selected predictors (basically P, ET, and TWS) were systematically plotted and evaluated in relation to each other. This analysis enables the assessment of their temporal evolution and variations. Subsequently, the focus shifts toward the prediction of soil moisture, a task accomplished via the application of the MLR model. In the domain of prediction, linear regression remains a stalwart approach in the realm of statistical prediction within hydrology and climatology. Its application is well-established, particularly owing to its traditional nature and recognized utility. Predictive skill can be performed at 1, 3, or 6 months lead time; however, for the drought prediction, the predictive skill of the indicators such the Standardized Precipitation Index (SPI), the standardized SSI, and the Multivariate Standardized Drought Index (MSDI) gradually decayed with the increasing lead time (Wang *et al.* 2020). A basic formulation of the MLR model for hydroclimatic variables prediction with respect to two predictors X and Z can be expressed at 1 month lead as shown in Equation 1:

$$Y_t = AX_{t-1} + BZ_{t-1} + \varepsilon_t \quad (1)$$

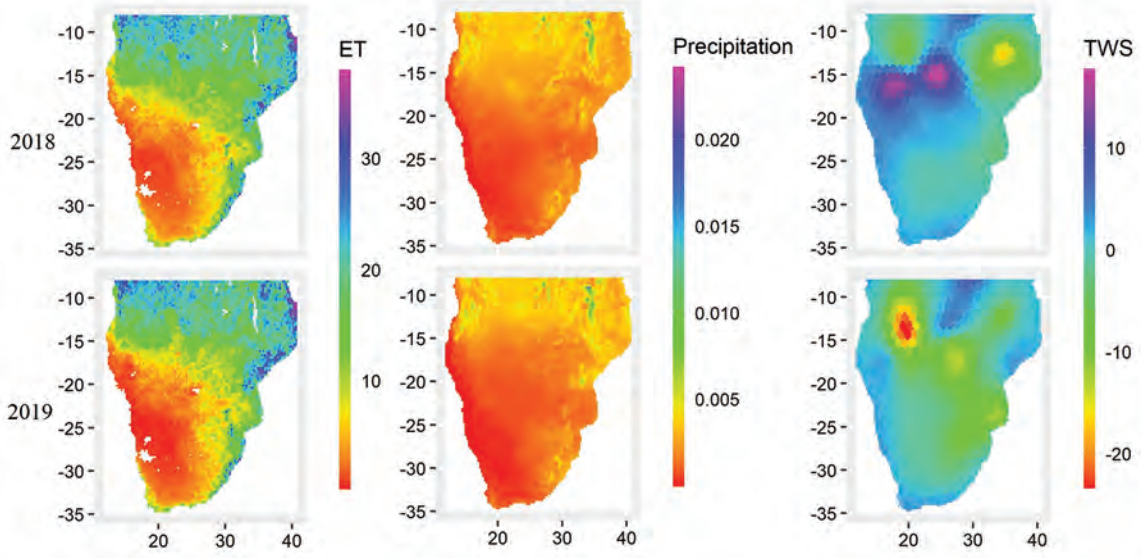

Figure 4. Original data with ranges: precipitation (m), evapotranspiration (ET) (mm), and total water storage (TWS) (cm).

where Y_t is the predictand (or dependent variable) in the form of soil moisture series (considered as drought indicator in this study), X_{t-1} and Z_{t-1} are covariates (or independent variables) that provide the predictive information of Y_t, A and B are regression coefficients, and ε_t is the error term.

Through the application of linear regression, a fundamental relationship emerges between the predicted variable (here soil moisture) and other influential variables, often referred to as predictors. This relationship serves to furnish valuable predictive insights into the development of soil moisture. In order to obtain the values of the constant (0.068) and coefficients (13.53, 0.004, and −0.0003) for precipitation (P), ET, and TWS, respectively, 100 random points were sampled from each monthly image. Only those points with valid values for each month and all the used parameters were selected. In the final step, MLR was calculated between the reference data (GLDAS) and the influencing parameters, namely, P, ET, and TWS. In essence, the regression model encapsulates the interplay between the anticipated soil moisture and a spectrum of predictors (P, ET, and TWS) encapsulated within Equation 2:

$$SM_{est} = 0.068 + 13.53P + 0.004ET - 0.0003TWS \quad (2)$$

In this formula, SM_{est} denotes the predicted soil moisture, P signifies precipitation, ET represents evapotranspiration, and TWS encapsulates the total water storage. Given the negligible effect of TWS, a simplified rendition of the formula takes the following form:

$$SM_{est} = 0.068 + 13.53P + 0.004ET \quad (3)$$

It is noteworthy that the MLR method's consistency in generating reliable outcomes persists across varying time spans of input data. To discern their relative significance in influencing soil moisture deficits, a careful analysis of the regression coefficients highlights the contribution of each factor. In this context, precipitation emerges as the most pivotal variable, significantly shaping soil moisture alterations, followed by evapotranspiration. Conversely, the contribution of TWS remains notably insignificant, which may be due to its delay in response to soil moisture variations. For instance, Houborg *et al.* (2012) noted that integrating GRACE TWS data into their catchment land surface model yielded no statistically significant enhancement in soil moisture estimates.

Second, the comparative analysis of SMAP and CYGNSS soil moistures vis-à-vis other soil moisture data sets followed a comprehensive methodology. Initially, box plots and histograms are used to delineate the distribution of data across the variables. Subsequently, soil moistures are plotted on a temporal evolution basis to depict their changes in temporal variations. Furthermore, scatter plots are used to visually illustrate the relationships between variables, complemented by the computation of Pearson correlations for quantitative insights.

Last, the validation of SMAP and CYGNSS soil moistures are used to find the alignment with the Southern Africa drought map (GDACS 2020) considered as the ground truth data for the same temporal span. However, before all the data were brought to a common spatial resolution and to ensure data reliability, the effect of seasonality is factored out from the soil moisture readings. In fact, given the inherent differences in spatial and temporal resolutions among the data sets used in this study, the bilinear resampling method within R programming was applied to standardize all data sets to a consistent 1° × 1° spatial resolution. This method calculates a pixel's value by considering a weighted distance average from its four adjacent pixels. Following this resampling process, all data sets were further adjusted to a uniform monthly temporal resolution for further analysis. The effect of seasonality was removed from the data using Deseason function of Matlab in order to avoid leading to false correlations.

Results and Analysis

Temporal Variability of TWS, Precipitation, and ET

Figure 4 represents the original data with ranges, and Figure 5 shows the temporal variations of TWS, Precipitation, and ET. As can be seen,

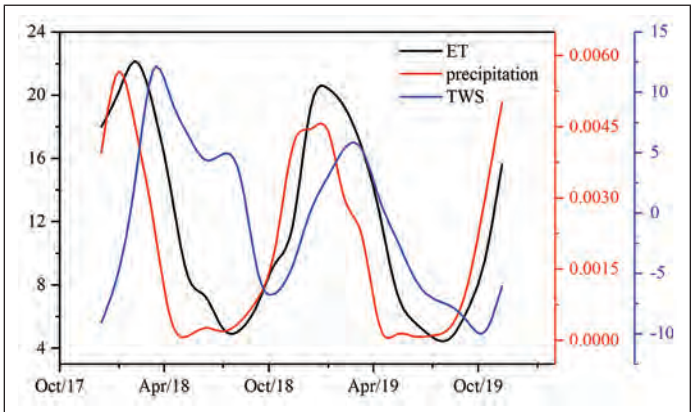

Figure 5. Temporal variations in change of total water storage (TWS) (cm), precipitation (m) and evapotranspiration (ET) (mm).

the variables follow each other on temporal basis, even though shifts are observed, especially, with TWS. The observed shifts could be attributed to several factors related to hydrological and meteorological processes. For instance, it takes time for precipitation to infiltrate into the soil and contribute to groundwater storage (TWS). Similarly, the effect of changes in ET on TWS might not be immediately apparent due to varying rates of evapotranspiration in different regions. Moreover, the interplay between precipitation, ET, and TWS depends on the hydrological connectivity of the region and local topography. Some areas might have rapid drainage systems that respond quickly to precipitation, while others might have slower drainage, leading to delayed responses in TWS. Groundwater recharge and discharge systems often act as buffers, storing water for longer periods. Changes in precipitation and ET can affect groundwater recharge and discharge rates, leading to shifts in TWS that might not directly correspond to precipitation patterns. In addition, different seasons and large-scale climate oscillations can exhibit distinct patterns of precipitation and ET. Seasonal variations in vegetation growth and ET rates can affect the overall water balance and consequently affect TWS.

To pinpoint the exact cause of the observed shifts, it is important to analyze the local hydrological conditions, land characteristics, and other relevant factors specific to the study area. Incorporating more data, conducting detailed hydrological modeling, and considering additional variables could help provide a clearer understanding of the reasons behind the observed shifts.

Figure 6 represents the MLR-predicted soil moisture depicting pronounced seasonal evolution and variation. The oscillations are evident with minimal and maximal soil moisture values between 0.12 and 0.24, respectively, for both years. MLR soil moisture and the predictors temporal variations approximately fit well, illustrating the reliability of the method used. To validate the result, MLR soil will, in turn, be compared with the reference soil moisture (GLDAS) and together with SMAP and CYGNSS soil moisture.

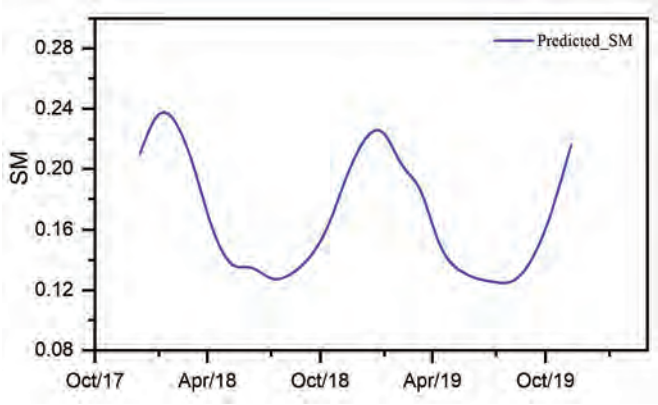

Figure 6. Temporal evolution of multiple linear regression (MLR) estimate soil moisture (SM) (m^3/m^3).

Box Plots and Histograms of the Soil Moistures

Figure 7 presents a box plot that effectively portrays the distribution characteristics of the SMAP, CYGNSS, GLDAS, and predicted SM data sets. The box plot provides a comprehensive depiction of the central tendency, spread, and outliers of the data. The central segment of the box corresponds to the median, signifying the point where 50% of the data resides. The median line traversing the box demonstrates the distribution of data values relative to this median. The whiskers, extending both upward and downward, capture data values lying beyond the median, offering insights into the data's dispersion. The interquartile range (IQR), delineated by the span from the 1st quartile (Q1) to the 3rd quartile (Q3), showcases the extent of data scattering between each sample. The length of the box is indicative of data dispersion, with a lengthier box implying greater dispersion, while a compact box signifies less divergence among data points.

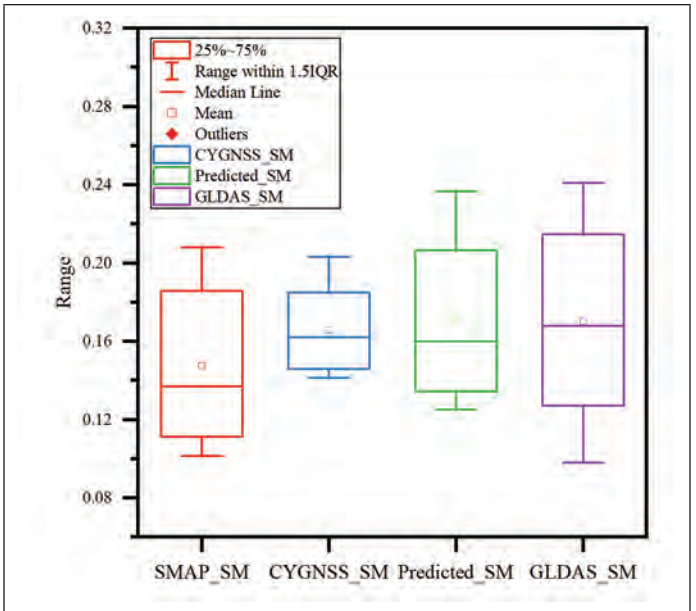

Figure 7. Boxes plots of Soil Moisture Active Passive (SMAP) (m^3/m^3), Cyclone Global Navigation Satellite System (CYGNSS) (cm^3/cm^3), multiple linear regression (MLR) predicted (m^3/m^3), and Global Land Data Assimilation System (GLDAS) (m^3/m^3) soil moistures. IQR = interquartile range.

Figure 8 features histogram plots, shedding light on the frequency distribution of soil moistures. These histograms illustrate that a substantial concentration of counts predominantly aligns on the lower left side, below the soil moisture value of 0.2, denoting a propensity for drier conditions. Notably, the entire ensemble of figures exhibits a distinct right-skewed distribution, underscoring a trend in which values are concentrated toward the lower end of the scale with a tail extending to the right. Overall these distribution characteristics of soil moisture data can help in drought prediction.

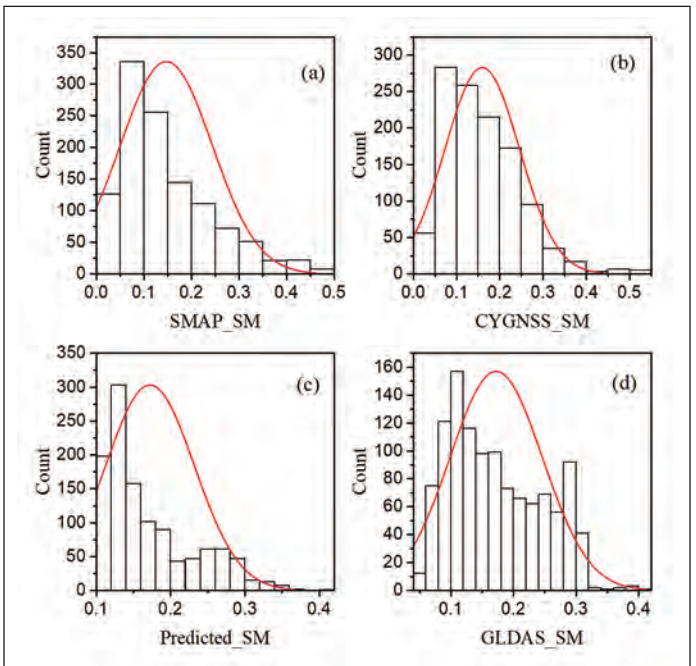

Figure 8. Histogram of Soil Moisture Active Passive (SMAP), Cyclone Global Navigation Satellite System (CYGNSS), multiple linear regression (MLR)−predicted, and Global Land Data Assimilation System (GLDAS) soil moistures.

Temporal Evolution of Different Soil Moistures

To assess the credibility of SMAP and CYGNSS SM data, a comparative analysis is conducted against both the predicted and reference SM data sets. Figure 9 vividly captures the temporal dynamics of these data sets, revealing distinctive characteristics within their variations. Notably, discernible oscillations are evident in the predicted and GLDAS data, both exhibiting analogous patterns of variability. In contrast, the SMAP and CYGNSS data manifest a marked divergence from this trend. While the maximum SM values of SMAP and CYGNSS align closely, it is noteworthy that SMAP displays an intriguing behavior by offering consistently lower minimum values. In fact, SMAP's minimum values extend to a remarkable extent, mirroring the minima observed in the GLDAS data set. This nuanced behavior underscores SMAP's capacity to capture not only elevated SM values but also the lower extremes, encompassing the range of variability spanned by the GLDAS reference data set. This capacity may be explained by the data quality and the measurement methods. Certain data sets exhibit more pronounced seasonal variations, and this difference in variation illustrates their capability in drought monitoring and prediction.

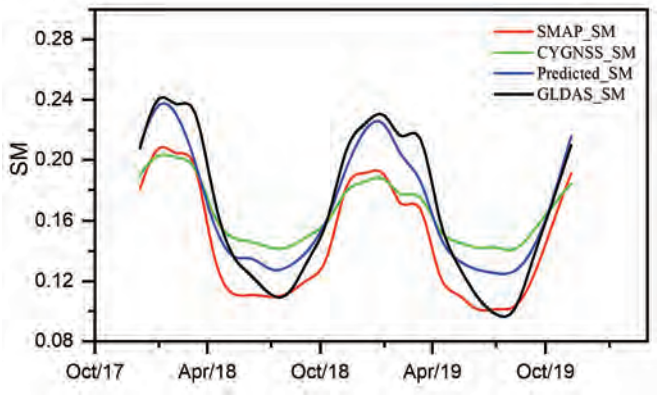

Figure 9. Temporal evolution of Soil Moisture Active Passive (SMAP) (m^3/m^3), Cyclone Global Navigation Satellite System (CYGNSS) (cm^3/cm^3), Global Land Data Assimilation System (GLDAS) (m^3/m^3), and the predicted soil moistures (SM) (m^3/m^3).

Pearson Correlations Between Different Soil Moistures

Figure 10 shows the scatter plots and Pearson correlations (r) between different soil moistures with $r = 0.78$, $r = 0.61$, and $r = 0.84$ between GLDAS and SMAP, GLDAS and CYGNSS, and GLDAS and the estimated SM, respectively, as reported in Table 2. These strong or moderate correlations signify in terms of the reliability and accuracy of SMAP, CYGNSS, and MLR-predicted soil moisture data in relation to the reference data set (GLDAS). As can be seen, MLR SM against GLDAS exhibits strong correlation, followed by SMAP and GLDAS, and last CYGNSS and GLDAS. The degree of consistency of the correlations implies the reliability of the data sets and their capability in drought monitoring and prediction.

Table 2. Pearson correlation (r).

	GLDAS SM
SMAP SM	0.78
CYGNSS SM	0.61
MLR SM	0.84

CYGNSS = Cyclone Global Navigation Satellite System; GLDAS = Global Land Data Assimilation System; MLR = multiple linear regression; SM = soil moisture; SMAP = Soil Moisture Active Passive.

Validation of SMAP and CYGNSS Soil Moistures

Figure 11 offers a compelling exploration of the spatial progression of both arid and humid conditions, presenting a side-by-side comparison of SMAP and CYGNSS SM spatial maps with those of GLDAS and the projected SM for 2018 and 2019. The insight derived from these visualizations is pivotal for understanding the convergence and divergence in spatial distribution. In tandem with this, Figure 12 presents the FAO drought map, which serves as a referential baseline representing authentic values. Monthly rainfall, maximum dry spell in the month, date of start of the growing season (SoS), NDVI (monthly average), and LST (monthly average) are the variables used and weighted to obtain the drought map, which is some form of anomaly of the standardized variable. Strikingly, a coherent pattern emerges, closely aligning the FAO drought map with the spatial depiction of the study period. Notably, as one delves into the comparative analysis of these spatial maps, a distinct spatial distinction becomes evident, revealing the accentuation of dry conditions within the southwestern regions in contrast to other locales.

Discussion

The three key explanatory variables (precipitation, ET, and TWS) exhibit robust autocorrelation (see Figure 5), underscoring their reliability in predicting soil moisture, which demonstrated its reliability in drought predictions for this study. Noteworthy shifts identified in TWS behavior can be attributed to the sensitivity of groundwater to prolonged dry periods. A deeper exploration reveals that GRACE TWS exhibits gradual variations, in contrast to the swift responsiveness of soil moisture to atmospheric dynamics.

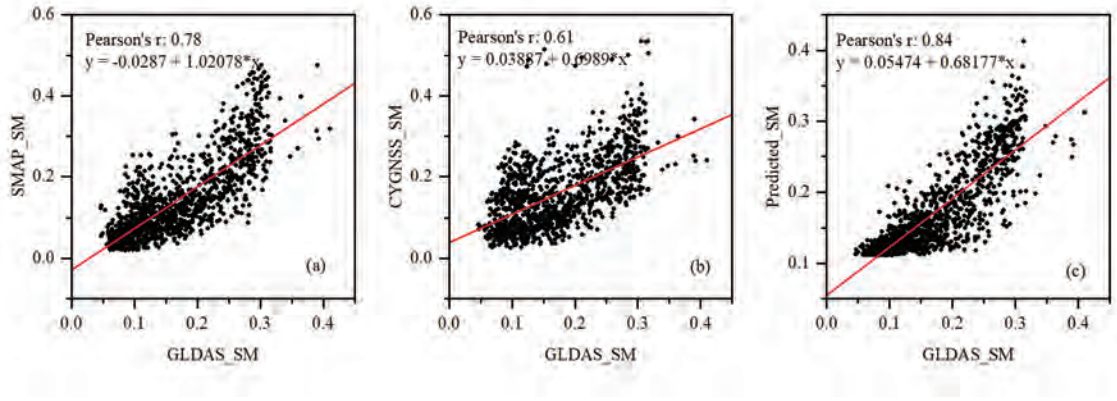

Figure 10. Scatter plots and correlation between: (a) Soil Moisture Active Passive (SMAP) (m^3/m^3) and Global Land Data Assimilation System (GLDAS) (m^3/m^3). (b) Cyclone Global Navigation Satellite System (CYGNSS) (cm^3/cm^3) and GLDAS (m^3/m^3). (c) Multiple linear regression (MLR)–predicted soil moistures (SM) (m^3/m^3) and GLDAS (m^3/m^3).

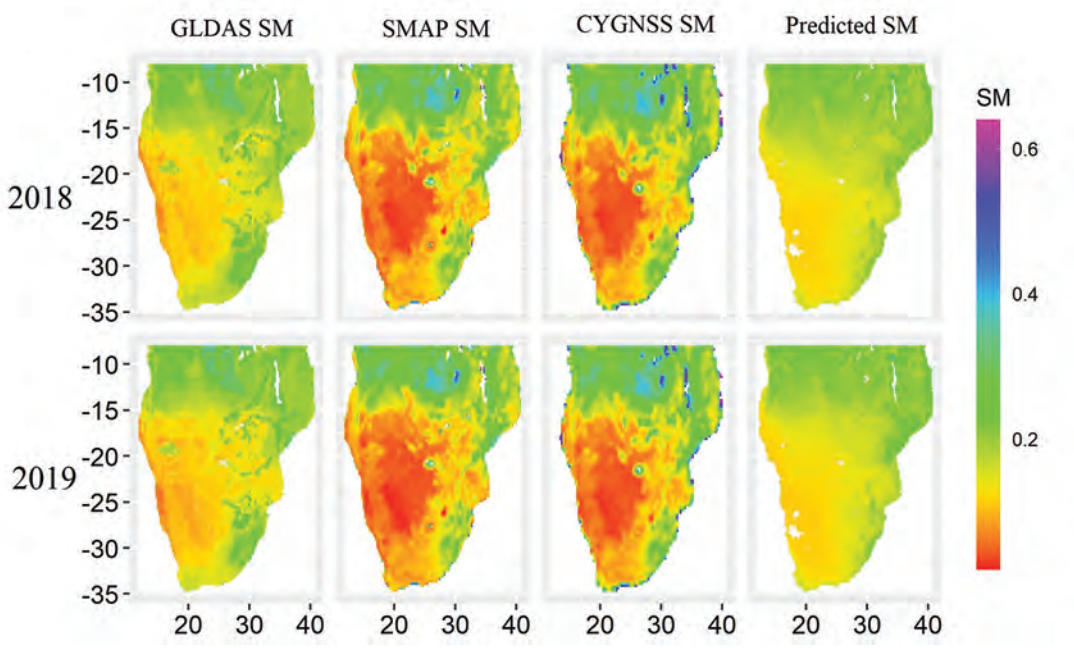

Figure 11. Spatial maps of Soil Moisture Active Passive (SMAP) (m^3/m^3), Cyclone Global Navigation Satellite System (CYGNSS) (cm^3/cm^3), Global Land Data Assimilation System (GLDAS) (m^3/m^3), and multiple linear regression (MLR)–predicted soil moistures (SM) (m^3/m^3).

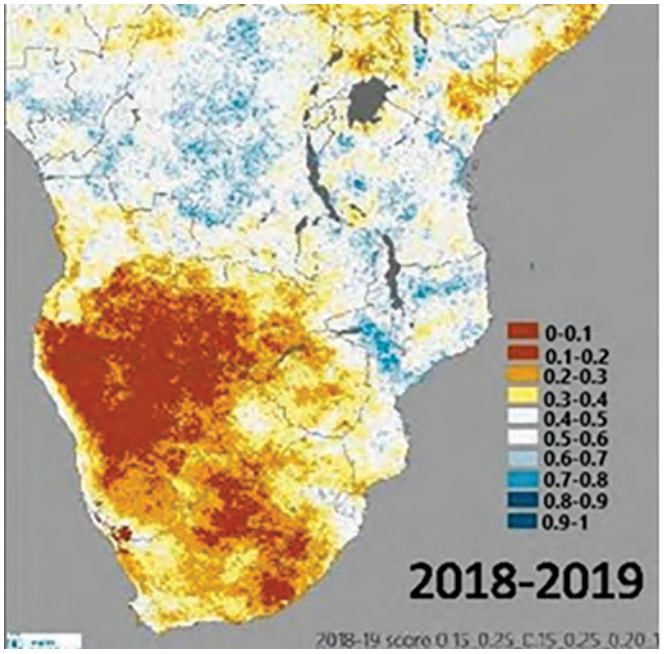

Figure 12. Reference map of drought spatial distribution of Southern Africa of the year 2018–2019 (GDACS 2020).

The drought indicators used (namely, precipitation and ET) hold sensitivity to transient dry conditions, enabling their effective use in soil moisture estimation. The congruence in spatial and seasonal trends between the estimated soil moisture and other data sets underscores its validity. Using the MLR approach to forecast soil moisture change (a critical variable for agricultural drought monitoring and prediction) yielded favorable outcomes. The MLR technique effectively captures the intricate interplay of inputs and outputs, reflecting the hydrophysical quantity of soil moisture deficit, encapsulating elements such as precipitation, evapotranspiration, infiltration, and runoff.

Figure 9 illuminates the temporal profiles of SMAP, CYGNSS, GLDAS, and the estimated soil moisture, revealing an admirable alignment that underscores the precision of the MLR model. This synchronization further extends to SMAP and CYGNSS soil moistures, signifying their potential as pivotal parameters for drought prediction, especially when corroborated against the reference data set, GLDAS usually used in drought prediction. Additionally, the graphical representations (box plots and histograms) unveil an overall normal data distribution, albeit with certain disparities discerned in SMAP and estimated soil moisture distributions.

Figure 10 accentuates this narrative through scatter plots and Pearson correlation coefficients (r). Impressively robust correlation coefficients (r = 0.78 between GLDAS and SMAP, r = 0.61 between GLDAS and CYGNSS, and r = 0.84 between GLDAS and predicted SM) fortify the credibility of the soil moisture data, particularly the predicted variant against the reference.

Spatial appraisal of variables from 2018 to 2019 demonstrates uniform patterns during this period (see Figure 11), corroborated even against the Southern African drought map of the same period (see Figure 12). The prevalence of dry conditions in southwest regions stems directly from precipitation deficits, a well-acknowledged driving factor. Evident from the histograms (see Figure 8), soil moisture values below 0.2 amass on the left side, indicative of the arid conditions that characterized the study area during this period. This arrangement accounts for the right-skewed nature of the histograms. Notably, the spatial mapping indicates that calculations at each grid cell are independent, further enhancing the robustness of the analysis.

Conclusions

This study underscores the valuable contributions of SMAP and CYGNSS soil moistures in the realm of drought prediction, particularly in the context of short-term dry conditions. The comprehensive assessment and comparison of SMAP and CYGNSS with other data sets reveal not only similar spatiotemporal patterns but also robust correlations, solidifying their relevance in drought prediction efforts. Consequently, leveraging SMAP and CYGNSS soil moisture data for forecasting dry conditions emerges as a logical and effective strategy.

The utility of accurately predicted dry conditions is undeniably significant, offering a pivotal tool to facilitate informed decision-making and proactive mitigation strategies, especially in the lead-up to crucial growing seasons. However, it is vital to acknowledge that soil moisture, a pivotal indicator for agricultural drought, exhibits pronounced spatiotemporal variability. This intricacy poses certain limitations on the precision of change predictions, especially under extreme conditions. Consequently, predicting these nuanced parameters remains a notable challenge. Furthermore, the development of drought is characterized by a gradual progression, a stark contrast to the rapid onset of events like floods and hurricanes. This intrinsic nature of drought complicates its early identification and prediction, making it an intricate task that requires meticulous analysis and robust methodologies. Additionally, the multifaceted hydrological processes inherent to drought further elevate the complexity of prediction endeavors.

In culmination, this study serves as a compelling testament to the reliable capabilities of SMAP and CYGNSS in both monitoring and predicting drought events. The insights garnered from spatial mapping distinctly underscore SMAP's heightened sensitivity to drought conditions, closely pursued by CYGNSS. As the field of drought prediction continues to evolve, the integration of advanced technologies and methodologies such as those used here will undoubtedly contribute to enhancing our understanding and proactive management of this critical natural phenomenon.

Acknowledgments

This work was supported by Jiangsu Marine Science and Technology Innovation Project (Grant No. JSZRHYKJ202202). The authors thank ESA and NASA for providing the data.

References

Ainembabazi, J.H., 2018. "The 2015-16 El Niño-induced drought crisis in Southern Africa: What do we learn from historical data?," 2018 Conference, July 28-August 2, 2018, Vancouver, British Columbia 275952, International Association of Agricultural Economists.

Barros, A. P. and G. J. Bowden. 2008. Toward long-lead operational forecasts of drought: An experimental study in the Murray-Darling River Basin. *Journal of Hydrology 357*(3–4):349–367.

Beaudoing, H. and M. Rodell. 2019. NASA/GSFC/HSL, GLDAS Noah Land Surface Model L4, version 2.0, https://doi.org/10.5067/9SQ1B3ZXP2C5.

Bourdin, D. R., S. W. Fleming and R. B. Stull. 2012. Streamflow modelling: A primer on applications, approaches and challenges. *Atmosphere-Ocean* 50(4):507–536.

Calabia, A., I. Molina and S. G. Jin. 2020. Soil moisture content from GNSS reflectometry using dielectric permittivity from fresnel reflection coefficients. Remote Sensing 12(1):122. https://doi.org/10.3390/rs12010122.

CYGNSS. 2020. UCAR-CU CYGNSS level 3 soil moisture version 1.0. https://doi.org/10.5067/CYGNU-L3SM1.

Dai, A. 2011. Drought under global warming: A review. *Wiley Interdisciplinary Reviews: Climate Change* 2(1):45–65.

Edokossi, K., A. Calabia, S. G. Jin and I. Molina. 2020. GNSS-reflectometry and remote sensing of soil moisture: A review of measurement techniques, methods and applications. *Remote Sensing* 12(4):614. https://doi.org/10.3390/rs12040614.

Elameen, A., S. G. Jin and D. Olago. 2023. Identification of drought events in major basins of Africa from GRACE total water storage and modeled products. *Photogrammetric Engineering and Remote Sensing* 89(4):221–232. https://doi.org/10.14358/PERS.22-00092R2.

Entekhabi, D., E. G. Njoku, P. E. O'Neill, K. H. Kellogg, W. T. Crow, W. N. Edelstein, J. K. Entin, S. D. Goodman, T. J. Jackson, J. Johnson, J. Kimball, J. R. Piepmeier, R. D. Koster, N. Martin, K. C. McDonald, M. Moghaddam, S. Moran, R. Reichle, J. C. Shi, M. W. Spencer, S. W. Thurman, L. Tsang and J. Van Zyl. 2010. The soil moisture active passive (SMAP) mission. *Proceedings of the IEEE 98*(5). https://doi.org/10.1109/JPROC.2010.2043918.

Entekhabi, D., N. Das, E. G. Njoku, J. T. Johnson and J. Shi. 2016. SMAP L3 radar/radiometer global daily 9 km EASE-grid soil moisture, version 3. https://doi.org/10.5067/7KKNQ5UURM2W.

Eswar, R., N. N. Das, C. Poulsen, A. Behrangi, J. Swigart, M. Svoboda, D. Entekhabi, S. Yueh, B. Doorn and J. Entin. 2018. SMAP soil moisture change as an indicator of drought conditions. *Remote Sensing* 10(5). https://doi.org/10.3390/rs10050788.

Evans, J. P., X. Meng and M. F. McCabe. 2017. Land surface albedo and vegetation feedbacks enhanced the millennium drought in south-east Australia. *Hydrology and Earth System Sciences* 21(1):409–422.

Fahimi, F., Z. M. Yaseen and A. El-shafie. 2017. Application of soft computing based hybrid models in hydrological variables modeling: A comprehensive review. *Theoretical and Applied Climatology* 128:875–903.

Ganguli, P.and M. J. Reddy. 2014. Ensemble prediction of regional droughts using climate inputs and the SVM–copula approach. *Hydrological Processes* 28(19):4989–5009.

GDACS. 2020. FAO in the 2019 humanitarian appeal: 2018/19 El Niño Response Plan for Southern Africa - Zimbabwe. www.gdacs.org. Accessed 10 Sept. 2021

Hao, Z., V. P. Singh and Y. Xia. 2018. Seasonal drought prediction: Advances, challenges and future prospects. *Reviews of Geophysics* 56(1). https://doi.org/10.1002/2016RG000549.

Heki, K. and S. G. Jin. 2023. Geodetic study on earth surface loading with GNSS and GRACE. *Satellite Navigation* 4(2):24. https://doi.org/10.1186/s43020-023-00113-6.

Houborg, R., M. Rodell, B. Li, R. Reichle and B. F. Zaitchik. 2012. Drought indicators based on model-assimilated Gravity Recovery and Climate Experiment (GRACE) terrestrial water storage observations. *Water Resources Research* 48(7). https://doi.org/10.1029/2011WR011291.

Huang, M. and S. G. Jin. 2020. Rapid flood mapping and evaluation with a supervised classifier and change detection in Shouguang using *Sentinel-1* SAR and *Sentinel-2* optical data. *Remote Sensing* 12(13):2073. https://doi.org/10.3390/rs12132073.

Hwang, Y. and G. J. Carbone. 2009. Ensemble forecasts of drought indices using a conditional residual resampling technique. *Journal of Applied Meteorology and Climatology* 48(7):1289–1301.

Jin, S.G., G. Feng and S. Gleason. 2011. Remote sensing using GNSS signals: current status and future directions. *Advances in Space Research* 47(10):1645–1653, https://doi.org/10.1016/j.asr.2011.01.036.

Jin, S. G. and T. Zhang. 2016. Terrestrial water storage anomalies associated with drought in Southwestern USA derived from GPS observations. *Surveys in Geophysics* 37(6):1139–1156. https://doi.org/10.1007/s10712-016-9385-z.

Johannesburg Regional Bureau. 2020. Southern Africa: Seasonal overview and drought hotspot analysis (2019/2020). https://docs.wfp.org/api/documents/WFP-0000115666/download/?iframe. Accessed 10 Sept. 2021

Jung, C., Y. Lee, Y. Cho and S. Kim. 2017. A study of spatial soil moisture estimation using a multiple linear regression model and MODIS land surface temperature data corrected by conditional merging. *Remote Sensing* 9(8). https://doi.org/10.3390/rs9080870

Khedun, C. P., A. K. Mishra, V. P. Singh and J. R. Giardino. 2014. A copula-based precipitation forecasting model: Investigating the interdecadal modulation of ENSO's impacts on monthly precipitation. *Water Resources Research* 50(1):580–600.

Koster, R. D., A. K. Betts, P. A. Dirmeyer, M. Bierkens, K. E. Bennett, S. J. Déry, J. P. Evans, R. Fu, F. Hernandez, L. R. Leung, M. Masood, H. Savenije, G. Wang and X. Yuan. 2017. Hydroclimatic variability and predictability: A survey of recent research. *Hydrology and Earth System Sciences* 21(7):3777–3798.

Koster, R. D., P. A. Dirmeyer, Z. Guo, G. Bonan, E. Chan, P. Cox, C. T. Gordon, S. Kanae, E. Kowalczyk, D. Lawrence, P. Liu, C.-H. Lu, S. Malyshev, B. McAvaney, K. Mitchell, D. Mocko, T. Oki, K. Oleson, A. Pitman, Y. C. Sud, C. M. Taylor, D. Verseghy, R. Vasic, Y. Xue, T. Yamada, and GLACE Team. 2004. Regions of strong coupling between soil moisture and precipitation. *Science* 305(5687):1138–1140.

Lawal, S., C. Lennard and B. Hewitson. 2019. Response of southern African vegetation to climate change at 1.5 and 2.0 global warming above the pre-industrial level. *Climate Services* 16:100134.

Lawrimore, J., R. R. Heim Jr, M. D. Svoboda, V. Swail and P. J. Englehart. 2002. Beginning a new era of drought monitoring across North America. *Bulletin of the American Meteorological Society* 83(8):1191–1192.

Liu, Y. and Y. Hwang. 2015. Improving drought predictability in Arkansas using the ensemble PDSI forecast technique. *Stochastic Environmental Research and Risk Assessment* 29:79–91.

Liu, W. T. and R. I. N. Juárez. 2001. ENSO drought onset prediction in northeast Brazil using NDVI. *International Journal of Remote Sensing* 22(17):3483–3501.

Maity, R., M. Suman and N. K. Verma. 2016. Drought prediction using a wavelet based approach to model the temporal consequences of different types of droughts. *Journal of Hydrology* 539:417–428.

Marsh, T. 2007. The 2004–2006 drought in southern Britain. *Weather* 62(7):191–196.

Mishra, A. K. and V. R. Desai. 2006. Drought forecasting using feed-forward recursive neural network. *Ecological Modelling* 198(1–2):127–138.

Mishra, A. K., V. R. Desai and V. P. Singh. 2007. Drought forecasting using a hybrid stochastic and neural network model. *Journal of Hydrologic Engineering* 12(6): 626–638.

Mishra, A. K. and V. P. Singh. 2010. A review of drought concepts. *Journal of Hydrology* 391(1–2):202–216.

Mishra, A., T. Vu, A. V. Veettil and D. Entekhabi. 2017. Drought monitoring with soil moisture active passive (SMAP) measurements. *Journal of Hydrology* 552:620–632.

MODIS. MODIS Evapotranspiration MOD16A2 Version 6 8-day. https://lpdaac.usgs.gov/products/mod16a2v006/

Morid, S., V. Smakhtin and K. Bagherzadeh. 2007. Drought forecasting using artificial neural networks and time series of drought indices. *International Journal of Climatology* 27(15):2103–2111.

Najibi, N. and S. G. Jin. 2013. Physical reflectivity and polarization characteristics for snow and ice-covered surfaces interacting with GPS signals. *Remote Sensing* 5(8):4006–4030. https://doi.org/10.3390/rs5084006.

Nicolai-Shaw, N., L. Gudmundsson, M. Hirschi and S. I. Seneviratne. 2016. Long-term predictability of soil moisture dynamics at the global scale: Persistence versus large-scale drivers. *Geophysical Research Letters* 43(16):8554–8562.

Nicolai-Shaw, N., J. Zscheischler, M. Hirschi, L. Gudmundsson and S. I. Seneviratne. 2017. A drought event composite analysis using satellite remote-sensing based soil moisture. *Remote Sensing of Environment* 203:216–225. https://doi.org/https://doi.org/10.1016/j.rse.2017.06.014

Nourani, V., A. H. Baghanam, J. Adamowski and O. Kisi. 2014. Applications of hybrid wavelet—Artificial intelligence models in hydrology: A review. *Journal of Hydrology* 514:358–377.

Ozger, M., A. K. Mishra and V. P. Singh. 2011. Estimating Palmer drought severity index using a wavelet fuzzy logic model based on meteorological variables. *International Journal of Climatology* 31(13):2021–2032.

Pinto, I. 2019. State of Climate in 2019 for Southern Africa. https://www.csag.uct.ac.za/2020/08/18/state-of-climate-in-2019-for-southern-africa/. Accessed 10 Sept. 2021

Panu, U. S. and T. C. Sharma. 2002. Challenges in drought research: Some perspectives and future directions. *Hydrological Sciences Journal* 47(S1): S19–S30.

Prakash, S., A. Sharma and S. S. Sahu. 2018. Soil moisture prediction using machine learning. *2018 Second International Conference on Inventive Communication and Computational Technologies (ICICCT)* 1–6. https://doi.org/10.1109/ICICCT.2018.8473260

Qian, X. and S. G. Jin. 2016. Estimation of snow depth from GLONASS SNR and phase-based multipath reflectometry. *IEEE Journal of Selected Topics in Applied Earth Observations and Remote Sensing* 9(10):4817–4823. https://doi.org10.1109/JSTARS.2016.2560763.

Qiu, Y., B. Fu, J. Wang and L. Chen. 2003. Spatiotemporal prediction of soil moisture content using multiple-linear regression in a small catchment of the Loess Plateau, China. *Catena* 54(1–2):173–195.

Qiu, Y., B. Fu, J. Wang, L. Chen, Q. Meng and Y. Zhang. 2010. Spatial prediction of soil moisture content using multiple-linear regressions in a gully catchment of the Loess Plateau, China. *Journal of Arid Environments* 74(2):208–220.

Relief Web. 2020. Special Report: Dry conditions for 2019–2020 season expected to continue across portions of Southern Africa. https://reliefweb.int/report/world/special-report-dry-conditions-2019-2020-season-expected-continue-across-portions. Accessed 10 Sept. 2021

Rhee, J. and J. Im. 2017. Meteorological drought forecasting for ungauged areas based on machine learning: Using long-range climate forecast and remote sensing data. *Agricultural and Forest Meteorology* 237:105–122.

Save, H., S. Bettadpur and B. D. Tapley. 2016. High resolution CSR GRACE RL05 mascons. *Journal of Geophysical Research: Solid Earth* 121(10):7547–7569. https://www2.csr.utexas.edu/grace/RL06_mascons.html. https://doi.org/10.1002/2016JB013007.

Schubert, S., R. Koster, M. Hoerling, R. Seager, D. Lettenmaier, A. Kumar and D. Gutzler. 2007. Predicting drought on seasonal-to-decadal time scales. *Bulletin of the American Meteorological Society* 88(10):1625–1630.

Seneviratne, S. I., T. Corti, E. L. Davin, M. Hirschi, E. B. Jaeger, I. Lehner, B. Orlowsky and A. J. Teuling. 2010. Investigating soil moisture–climate interactions in a changing climate: A review. *Earth-Science Reviews* 99(3–4):125–161.

Steinemann, A. C. and L. F. N. Cavalcanti. 2006. Developing multiple indicators and triggers for drought plans. *Journal of Water Resources Planning and Management* 132(3):164–174.

Su, H. and R. E. Dickinson. 2017. On the spatial gradient of soil moisture–precipitation feedback strength in the April 2011 drought in the Southern Great Plains. *Journal of Climate* 30(3):829–848.

Sun, L., S. W. Mitchell and A. Davidson. 2012. Multiple drought indices for agricultural drought risk assessment on the Canadian prairies. *International Journal of Climatology* 32(11):1628–1639.

Svoboda, M., D. LeComte, M. Hayes, R. Heim, K. Gleason, J. Angel, B. Rippey, R. Tinker, M. Palecki, D. Stooksbury, D. Miskus and S. Stephens. 2002. The drought monitor. *Bulletin of the American Meteorological Society* 83(8):1181–1190.

Thomas, A. C., J. T. Reager, J. S. Famiglietti and M. Rodell. 2014. A GRACE-based water storage deficit approach for hydrological drought characterization. *Geophysical Research Letters* 41(5). https://doi.org/10.1002/2014GL059323.

Tropical Rainfall Measuring Mission. 2011. TRMM (TMPA/3B43) rainfall estimate L3 1 month 0.25 degree x 0.25 degree V7, Greenbelt, MD, Goddard Earth Sciences Data and Information Services Center (GES DISC). https://doi.org/10.5067/TRMM/TMPA/MONTH/7.

Wang, W.-C., K.-W. Chau, C.-T. Cheng and L. Qiu. 2009. A comparison of performance of several artificial intelligence methods for forecasting monthly discharge time series. *Journal of Hydrology* 374(3–4):294–306.

Wang, Q. J., D. E. Robertson and F. H. S. Chiew. 2009. A Bayesian joint probability modeling approach for seasonal forecasting of streamflows at multiple sites. *Water Resources Research* 45(5). https://doi.org/10.1029/2008WR007355.

Wang, Y., J. Yang, Y. Chen, Z. Su, B. Li, H. Guo and P. De Maeyer. 2020. Monitoring and predicting drought based on multiple indicators in an arid area, China. *Remote Sensing* 12(14). https://doi.org/10.3390/rs12142298.

World Food Program. 2019. Southern Africa regional maize supply and market outlook. https://fscluster.org/sites/default/files/documents/sa_regional_supply_and_market_outlook_august_2019_to_march_2020.pdf.

Wu, L., D.-J. Seo, J. Demargne, J. D. Brown, S. Cong and J. Schaake. 2011. Generation of ensemble precipitation forecast from single-valued quantitative precipitation forecast for hydrologic ensemble prediction. *Journal of Hydrology* 399(3–4):281–298.

Xu, Y., L. Wang, K. W. Ross, C. Liu and K. Berry. 2018. Standardized soil moisture index for drought monitoring based on soil moisture active passive observations and 36 years of North American land data assimilation system data: A case study in the southeast United States. *Remote Sensing* 10(2). https://doi.org/10.3390/rs10020301

Yan, J., G.-Y. Liao, M. Gebremichael, R. Shedd and D. R. Vallee. 2012. Characterizing the uncertainty in river stage forecasts conditional on point forecast values. *Water Resources Research* 48(12):12509.

Yaseen, Z. M., A. El-Shafie, O. Jaafar, H. A. Afan and K. N. Sayl. 2015. Artificial intelligence based models for stream-flow forecasting: 2000–2015. *Journal of Hydrology* 530:829–844.

Yuan, X. and E. F. Wood. 2013. Multimodel seasonal forecasting of global drought onset. *Geophysical Research Letters* 40(18):4900–4905.

Zhu, Q., L. Luo, Y.-P. Xu, Y. Tian and T. Yang. 2019. Satellite soil moisture for agricultural drought monitoring: Assessment of SMAP-derived soil water deficit index in Xiang River Basin, China. *Remote Sensing* 11(3). https://doi.org/10.3390/rs11030362

Zink, M., L. Samaniego, R. Kumar, S. Thober, J. Mai, D. Schäfer and A. Marx. 2016. The German drought monitor. *Environmental Research Letters* 11(7):74002.